Received: 26 August 2021 | Revised: 12 December 2021 | Accepted: 16 December 2021

DOI: 10.1111/cas.15248

Cancer Science WILEY

ORIGINAL ARTICLE

Squalene synthase predicts poor prognosis in stage I-III colon adenocarcinoma and synergizes squalene epoxidase to promote tumor progression

Huihong Jiang[1,2] | Erjiang Tang[2,3] | Ying Chen[2,3] | Hailong Liu[1,2] | Yun Zhao[4,5,6] | Moubin Lin[1,2,3] | Luwei He[2,3]

[1]Department of General Surgery, School of Medicine, Yangpu Hospital, Tongji University, Shanghai, China

[2]Institute of Gastrointestinal Surgery and Translational Medicine, School of Medicine, Tongji University, Shanghai, China

[3]Center for Clinical Research and Translational Medicine, School of Medicine, Yangpu Hospital, Tongji University, Shanghai, China

[4]Hangzhou Institute for Advanced Study, School of Life Science, University of Chinese Academy of Sciences, Hangzhou, China

[5]The State Key Laboratory of Cell Biology, CAS Center for Excellence in Molecular Cell Science, Shanghai Institute of Biochemistry and Cell Biology, Chinese Academy of Sciences, University of Chinese Academy of Sciences, Shanghai, China

[6]School of Life Science and Technology, ShanghaiTech University, Shanghai, China

Correspondence
Yun Zhao, Hangzhou Institute for Advanced Study, School of Life Science, University of Chinese Academy of Sciences, 1 Xiangshan Branch Road, Hangzhou 310024, China.
Email: yunzhao@sibcb.ac.cn

Moubin Lin, Department of General Surgery, School of Medicine, Yangpu Hospital, Tongji University, 450 Tengyue Road, Shanghai 200090, China.
Email: 1500142@tongji.edu.cn

Luwei He, Institute of Gastrointestinal Surgery and Translational Medicine, School of Medicine, Tongji University, 450 Tengyue Road, Shanghai 200090, China.
Email: heluwei88@126.com

Funding information
National Natural Science Foundation of China, Grant/Award Number: 81874201; Shanghai Municipal Health Bureau, Grant/Award Number: ZK2019A19; Science and Technology Commission of Shanghai Municipality, Grant/Award Number: 19411971500; Shanghai Pujiang Program, Grant/Award Number: 21PJD066; National Key Research and

Abstract

Colon adenocarcinoma (COAD) is one of the most prevalent malignancies, with poor prognosis and lack of effective treatment targets. Squalene synthase (FDFT1) is an upstream enzyme of squalene epoxidase (SQLE) in cholesterol biosynthesis. In a previous study, we revealed that SQLE promotes colon cancer cell proliferation in vitro and in vivo. Here, we investigate the prognostic value of FDFT1 in stage I-III COAD and explore the potential underlying mechanisms. Squalene synthase was significantly upregulated in stage I-III COAD and positively correlated with poor differentiation and advanced tumor stage. High expression of FDFT1 was an independent predictor of overall and relapse-free survival, and the nomograms based on FDFT1 could effectively identify patients at high risk of poor outcome. Squalene synthase accelerated colon cancer cell proliferation and promoted tumor growth. Lack of FDFT1 resulted in accumulating NAT8 and D-pantethine to lower reactive oxygen species levels and inhibit colon cancer cell proliferation. Moreover, the combined inhibition of FDFT1 and SQLE induced a greater suppressive effect on cell proliferation and tumor growth than single inhibition. Taken together, these results indicate that FDFT1 predicts poor prognosis in stage I-III COAD and has the tumor-promoting effect on COAD through regulating NAT8 and D-pantethine. Targeting both FDFT1 and SQLE is a more promising therapy than their single inhibition for stage I-III COAD.

Abbreviations: APC, adenomatous polyposis coli; CEA, carcinoembryonic antigen; CI, confidence interval; COAD, colon adenocarcinoma; FDFT1, farnesyl-diphosphate farnesyltransferase 1 (squalene synthase); HR, hazard ratio; IHC, immunohistochemical; KD, knockdown; NAT8, *N*-acetyltransferase 8; OS, overall survival; RFS, relapse-free survival; ROS, reactive oxygen species; SQLE, squalene epoxidase; SREBP, sterol regulatory element-binding protein; TMA, tissue microarray.

Huihong Jiang and Erjiang Tang contributed equally to this work.

Development Program of China, Grant/Award Number:2020YFA0509000, 2017YFA0503600

KEYWORDS
colon adenocarcinoma, prognostic marker, squalene epoxidase, squalene synthase, tumor progression

1 | INTRODUCTION

Colon adenocarcinoma is one of the most common cancers, with high morbidity and mortality rates worldwide.[1-3] Surgery is the mainstay of treatment for patients with stage I-III COAD; however, 25%-40% of the patients will develop recurrence or metastasis even after curative resection.[4,5] To date, TNM classification represents the main prognostic tool for COAD patients undergoing radical surgery; however, its predictive accuracy is unsatisfactory.[6]

Dysregulation of translation, notably its progressive upregulation, is a key driver in the pathogenesis of COAD, and is closely associated with cancer metabolism, malignant progression, and therapeutic interventions.[7,8] Although quite a few gene expression signatures have been proposed for prognostic evaluation of COAD patients, such as the consensus molecular subtypes, they are difficult to integrate with the current staging system.[9] Thus, enhancing efficiency of prognostic prediction and exploring novel therapeutic targets are urgently needed to improve the prognosis of localized COAD.

Targeting cholesterol biosynthesis has become a potential treatment for COAD. It has been reported that truncated APC selective inhibitor-1, TASIN-1, kills COAD cells with APC truncations rather than normal cells or cancer cells with WT APC. TASIN-1 inhibits cholesterol biosynthesis through targeting emopamil-binding protein and inactivating SREBP2 feedback.[10] Downregulation of SREBPs also alleviates colonic dysplasia and impedes initiation of COAD and tumor growth.[11,12] In addition, the cholesterol-lowering statins exert antineoplastic effects and augment the chemosensitivity of COAD through targeting 3-hydroxy-3-methylglutaryl-coenzyme A reductase (HMGCR).[13,14]

In the cholesterol biosynthesis pathway, FDFT1 (squalene synthase) plays a key regulatory role in directing the metabolite farnesyl pyrophosphate to produce sterol or nonsterol.[15-17] Squalene synthase is upregulated in many cancers, and could act as a potential biomarker and a new therapeutic target of correlative cancers.[18] Squalene synthase increases cholesterol content of lipid rafts, and attenuates proliferation and induces death of prostate cancer cells.[19] Moreover, in lung cancers, FDFT1 promotes metastasis through enhancing tumor necrosis factor-a receptor 1 at lipid rafts or stimulating the osteopontin/ERK pathway.[20,21]

In the present study, we systematically investigated the protein expression and prognostic significance of FDFT1 in stage I-III COAD. Then we investigated the function and mechanism of FDFT1 in promoting colon cancer cell proliferation, as well as investigating the possibility that dual inhibition of FDFT1 and SQLE has potential for COAD treatment.

2 | MATERIALS AND METHODS

2.1 | Reagents

D-pantethine (abs816989) was purchased from absin. Lapaquistat (HY-14925) and terbinafine (HY-17395A) were purchased from MCE. *N*-acetyl-L-cysteine (S0077) was purchased from Beyotime.

2.2 | Patients and samples

From January 2014 to July 2018, 233 tumor samples were obtained from 233 COAD patients who underwent radical surgery at Yangpu Hospital affiliated to Tongji University School of Medicine; 217 of the tumor samples were paired with adjacent normal tissues. One hundred twenty-four (53.2%) patients were men and 109 (46.8%) were women, with a mean age of 71 ± 10.6 years. Relevant clinicopathologic variables were abstracted from patients' medical records, including date of diagnosis, operative method, tumor location, differentiation grade, tumor stage, and preoperative serum CEA level. According to the TNM classification, 41 cases (17.6%) were stage I, 94 (40.3%) stage II, and 98 (42.1%) stage III. The follow-up information was obtained by clinic visit or telephone interview between May and July 2021. The study protocol was approved by the ethics committee of our institution (LL-2021-SCI-004) and informed consent was obtained from all patients.

2.3 | Tissue microarray and IHC analyses

A total of 450 samples were fixed by formalin, embedded in paraffin, and used for TMA construction. Tissue slides with paraffin sections were deparaffinized by xylene and ethanol and used for IHC analyses. Endogenous peroxidase activity was blocked with 3% H_2O_2 for 15 minutes at room temperature. For antigen retrieval, slides were heated in citrate buffer for 20 minutes. Nonspecific binding was blocked with 10% FBS in PBS for 15 minutes at 37°C. The slides were incubated with FDFT1 (1:200 dilution; Cat# 13128-1-AP; Proteintech), Ki-67 (1:5000 dilution; Cat# ab15580; Abcam) at 4°C overnight. The slides were incubated with biotin-conjugated secondary Ab using a general SP kit (Cat# SP-9000; ZSGB-BIO) and stained with the DAB substrate (Cat# SP-9000; ZSGB-BIO). The immunoreactivity of tested samples was scored for multiplying staining intensity (0-3) and positive cell proportion (1-4).

2.4 | Plasmids and stable cell line construction

Squalene synthase was cloned into pCDH-PURO vector (Cat# 46970; Addgene). The FDFT1 and SQLE shRNAs were constructed into pLKO.1-PURO vector (Cat# 8453; Addgene) with the following shRNA target sequences: FDFT1, 5′-ACTTGCTACAAGTATCTCAAT-3′; SQLE, 5′-GGTGTTGTGTTACAGTTAT-3′; and Scramble, 5′-CCTAAGGTTAAGTCGCCCTCG-3′.

HEK293T cells were cotransfected with viral vectors (pCDH and PLKO.1) and packaging plasmids (psPAX2/pMD2.G; Cat# 12259/12260; Addgene) by using Lipofectamine 3000 (Cat# L3000015; Invitrogen). Forty-eight hours after transfection, cell medium was filtered through a 0.45-μmol L^{-1} filter (Cat# PN4614; PALL). Cells were infected with virus for 48 hours, then selected with puromycin (Cat# A1113803; Gibco) to construct stable cell lines.

2.5 | RNA interference

Human FDFT1 siRNAs were obtained from Generay. The siRNA oligonucleotides were transfected by Lipofectamine RNAiMAX (Cat# 13778150; Invitrogen) following the manufacturer's instructions. The siRNA target sequences used in this research are siFDFT1-1, 5′- GGCGGUUCAUGGAGAGCAAUU -3′ and siFDFT1-2, 5′-CAGGUAUGUUAAGAAGUUAUU -3′.

2.6 | Cell culture

The human embryonic kidney cell line 293T and CRC cell lines DLD1, HCT116, LS174T, RKO, SW480, and SW620 were cultured in DMEM (Cat# 11995065; Invitrogen) supplemented with 10% FBS (Cat# 10091148; Gibco) and 1% penicillin/streptomycin (Cat# 15140122; Gibco). HT29, HCT15, LoVo, and Caco2 cells were cultured in RPMI-1640 medium (Cat# 11875093; Gibco) supplemented with 10% FBS and 1% penicillin/streptomycin. NCM460 cells were cultured in RPMI-1640 medium supplemented with 10% FBS, 20 ng/mL human epidermal growth factor (Cat# E4269; Sigma), and 1% penicillin/streptomycin. These cells were all incubated at 37°C with 5% CO_2. All cells were obtained from Shanghai Life Academy of Sciences cell library.

2.7 | RNA extraction and quantitative PCR analysis

Total RNA was extracted by using TRIzol reagent (Cat# 15596026; Invitrogen). Reverse transcription was carried out using RT master mix (Cat# RR036B; Takara) and real-time PCR was carried out by SYBR Green (Cat# RR091A; Takara) according to the manufacturer's instructions. The $2^{-\Delta\Delta Ct}$ method was used for data analysis. The primers for real-time PCR are as follows: FDFT1, 5′-TGTGACCTCTGAACAGGAGTGG-3′ and 5′-GCCCATAGAGTTGGCACGTTCT-3′; and β-actin, 5′-CACCATTGGCAATGAGCGGTTC-3′ and 5′-AGGTCTTTGCGGATGTCCACGT-3′.

2.8 | Western blot analysis

Cells were washed with PBS and RIPA buffer (Cat# P0013B; Beyotime), PMSF (ST506; Beyotime), and phosphatase inhibitor cocktail (Cat#P1050; Beyotime) were added. Total proteins were separated by SDS-PAGE and then transferred onto PVDF membranes (Cat# IPVH00010; Millipore). Membranes were incubated with primary Abs against FDFT1 (1:1000 dilution; Cat# 13128-1-AP; Proteintech), NAT8 (1:500 dilution; Cat# A7759; Abclonal), SQLE (1:1000 dilution; Cat# 12544-1-AP; Proteintech), Tubulin (1:5000 dilution; Cat# E7; DSHB), and β-actin (1:5000 dilution; Cat# AC026; Abclonal) after being blocked at 4°C. Proteins were visualized using an ECL system following incubation with the secondary Abs against Goat anti-Rabbit IgG (H + L) Cross-Adsorbed Secondary Antibody, HRP (Cat# G21234; Invitrogen), and Goat anti-Mouse IgG (H + L) Cross-Adsorbed Secondary Antibody, HRP (Cat# G21040; Invitrogen).

2.9 | Cell proliferation assay

Cells (1×10^3-5×10^3 cells/well) were seeded into 96-well plates, and cell proliferation was measured by counting cell numbers or using an Enhanced CCK-8 (Cat# C0043; Beyotime) for 3 days. Three independent experiments were carried out.

2.10 | EdU staining

Cells were seeded in 96-well plates for 48 or 72 hours, and cell proliferation was detected by a BeyoClick EdU-555 kit (C0075; Beyotime). Images of cells were captured by fluorescence microscopy.

2.11 | Cell cycle detection

Cells (5×10^5 cells) were washed with PBS and fixed with 70% cold ethanol overnight at 4°C. Then cells were stained with propidium iodide (Cat# C1052; Beyotime) and examined by flow cytometry (BD Accuri C6; Biosciences) at 488 nm. The data were analyzed by FlowJo software (BD Biosciences).

2.12 | Cell apoptosis assay

Cells (5×10^5 cells) were washed with PBS and stained with annexin V-FITC/propidium iodide (Cat# C1062L; Beyotime). Data were analyzed by BD Accuri C6 software (BD Biosciences).

2.13 | Colony formation assay

Cells (200 cells/well) were seeded in 6-well plates in triplicate and cultured for 10 days. Cell colonies were fixed with 4% paraformaldehyde for 10-15 minutes followed by staining with Crystal Violet Staining Solution (Cat# C0121; Beyotime).

2.14 | Detection of ROS level

Cells were washed with serum-free DMEM and stained with DCFH-DA (Cat# S0033; Beyotime) at 37°C for 30 minutes. The fluorescence was examined by Cytoflex flow cytometry (Beckman Coulter) or BD Accuri C6 at 488 nm. Data were analyzed by CytExpert software (Beckman Coulter) or FlowJo software.

2.15 | Cholesterol measurement

Cholesterol was extracted from cells by methanol and chloroform (vol/vol, 1:2) and measured by an Amplex Red cholesterol assay kit (Cat# A12216; Invitrogen) according to the manufacturer's instructions.

2.16 | Xenograft tumor formation

Six-week-old male nude mice (BALB/cA-nu/nu) were obtained from Shanghai Experimental Animal Center. These mice were maintained in a pathogen-free environment. Stable cell lines (1×10^6-5×10^6 cells in 0.1 mL PBS) were subcutaneously injected into the left flank of nude mice. Tumor size was measured by digital caliper every 3-5 days after 1 week. Tumor volume (V) was calculated according to the formula: V (mm^3) = 0.5 × length × $width^2$. The mice were killed by cervical dislocation before the volume of tumors reached 1000 mm^3. The tumors were then harvested and weighed. All animals were used in accordance with the guidelines of the Institutional Animal Care and Use Committee of the Institute of Biochemistry and Cell Biology.

2.17 | Statistical analysis

Statistical analyses of experiments and clinical samples were undertaken using GraphPad Prism (GraphPad), SPSS version 22.0 (IMB-SPSS), and EmpowerStats software (X&Y Solutions). Data are expressed as mean ± SEM or mean ± SD. Paired or unpaired Student's *t* tests were applied for comparison of two groups. Multiple group comparisons were analyzed by multiple *t* tests, one per row. Categorical variables were described as frequencies and percentages and compared using χ^2 tests.

The clinical end-points of this study included OS and RFS, which were defined as the interval from diagnosis to death and recurrence, respectively. The Kaplan-Meier survival curves and log-rank test were used for the univariate analysis. Hazard ratios and their 95% CIs were calculated by Cox proportional hazard model with stepwise selection to determine the independent prognostic factors. The nomograms for OS and RFS were then constructed based on the multivariate analysis, and the predictive accuracy was quantified with the AUC. Bootstraps with 1000 resamples were applied to these activities. A *P* value of less than .05 was considered statistically significant.

3 | RESULTS

3.1 | Squalene synthase upregulated in stage I-III COAD tissues and colon cancer cell lines

To investigate the expression of FDFT1 in COAD, we collected clinical samples, including 233 COAD tissues and 217 adjacent normal tissues, for TMA analysis. The IHC analysis showed that the expression of FDFT1 was significantly upregulated in COAD tissues compared to paired adjacent normal tissues (Figure 1A). Two hundred and thirty-three COAD patients were divided into high expression (≥4, 125 cases) and low expression groups (<4, 108 cases) based on the IHC score of FDFT1. As shown in Table 1 and Figure 1B-D, $FDFT1^{high}$ cases were more likely to be poorly differentiated or mucinous ($P = .030$), and progressively increased with advancing tumor stage (10.4%, 42.4%, and 47.2% in stage I, II, and III, respectively; $P = .007$ for trend) and rising levels of serum CEA (40.8%, 28.8%, and 30.4% across CEA ≤5, 5-15, and ≥15 ng/mL, respectively; $P < .001$ for trend). Notably, high expression of FDFT1 was closely associated with depth of invasion ($P = .007$), but not with lymph node metastasis ($P = .110$). In addition, no significant correlation was detected for age, gender, tumor location, or operative method (all $P > .05$).

Immunohistochemical staining of adjacent normal tissues and COAD tissues ($FDFT1^{low}$/$FDFT1^{high}$) is shown in Figure 1E. Consistent with these observations, we also found the expression of

FIGURE 1 Squalene synthase (FDFT1) was upregulated in stage I-III colon adenocarcinoma (COAD) tissues and colon cancer cell lines. A, Comparison of FDFT1 expression between 217 COAD and paired adjacent normal (AN) tissues from tissue microarray (TMA). B, Comparison of FDFT1 expression in different TNM stages (I-III) from TMA. C, Comparison of FDFT1 expression in different T stages (1-3, 4) from TMA. D, Comparison of FDFT1 expression in different differentiation grades (well/moderate, poor/mucinous) from TMA. Mean ± SD. E, FDFT1 expression in two paired AN and COAD tissues were detected by immunohistochemical analysis. $FDFT1^{low}$ and $FDFT1^{high}$ in COAD tissues are shown below. Scale bars, 50 μm. F, FDFT1 mRNA level in normal colon mucosal epithelial cells (NCM460) and colon cancer cell lines. NCM460 was used as control, housekeeping gene *ACTB* was used loading control. $^*P < .05$, $^{***}P < .001$

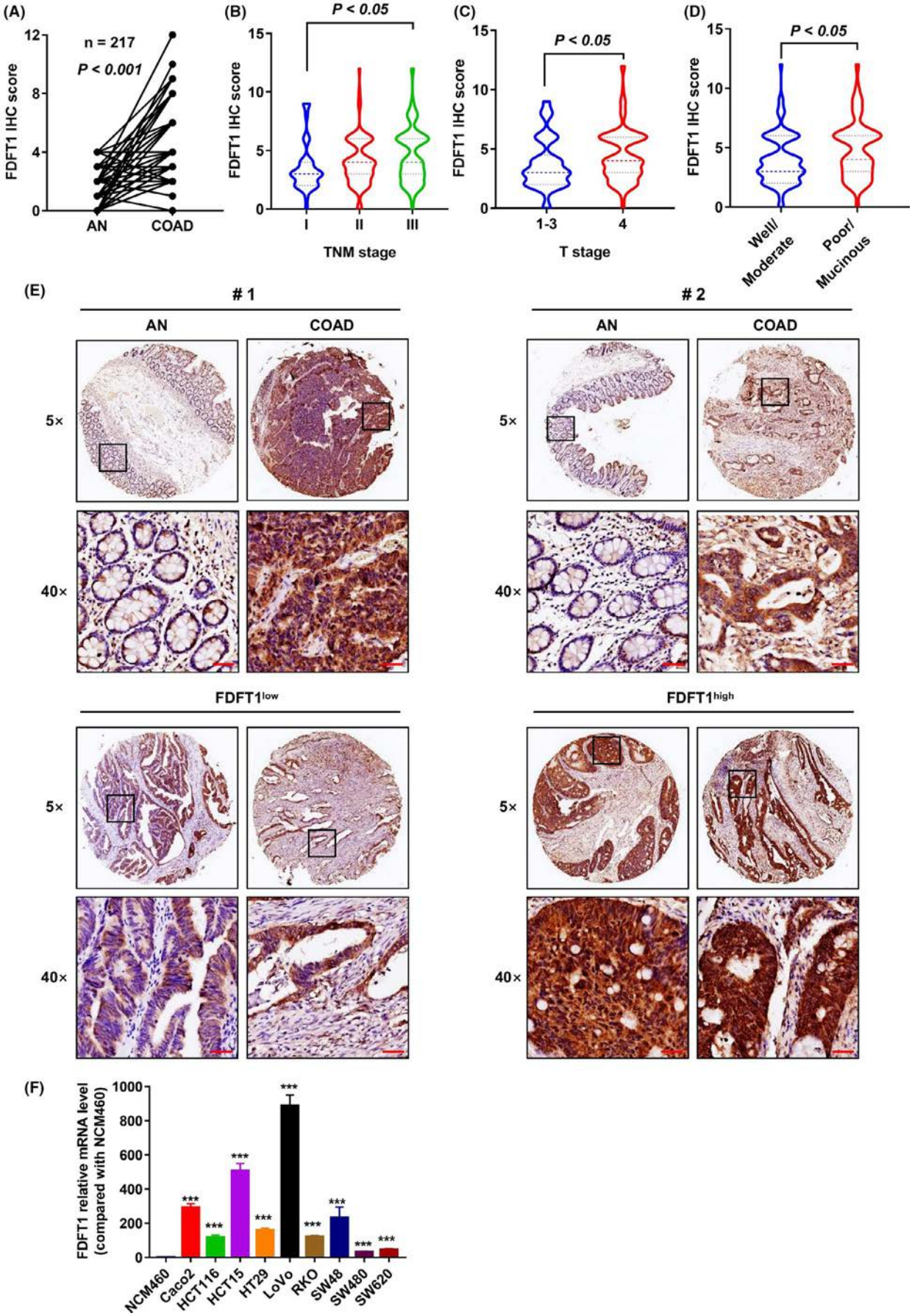
(A)
n = 217
P < 0.001
FDFT1 IHC score
AN
COAD
(B)
P < 0.05
FDFT1 IHC score
I
II
III
TNM stage
(C)
P < 0.05
FDFT1 IHC score
1-3
4
T stage
(D)
P < 0.05
FDFT1 IHC score
Well/ Moderate
Poor/ Mucinous
(E)
1
2
AN
COAD
5×
40×
FDFT1low
FDFT1high
(F)
FDFT1 relative mRNA level (compared with NCM460)
NCM460
Caco2
HCT116
HCT15
HT29
LoVo
RKO
SW48
SW480
SW620

TABLE 1 Comparison of clinicopathologic features of patients with stage I-III colon adenocarcinoma between low and high expression of squalene synthase (FDFT1)

Variable	Group	FDFT1^{low} (N = 108)	FDFT1^{high} (N = 125)	*P* value
Age (y); mean (range)		69 (47-94)	70 (46-91)	.267
Gender	Male	61 (56.5)	63 (50.4)	
	Female	47 (43.5)	62 (49.6)	.361
Tumor location	Right-sided	47 (43.5)	68 (54.4)	
	Left-sided	61 (56.5)	57 (45.6)	.115
Differentiation grade	Well/moderate	90 (83.3)	89 (71.2)	
	Poor/mucinous	18 (16.7)	36 (28.8)	.030
TNM stage	I	28 (25.9)	13 (10.4)	
	II	41 (38.0)	53 (42.4)	
	III	39 (36.1)	59 (47.2)	.007
T stage	1-3	50 (46.3)	36 (28.8)	
	4	58 (53.7)	89 (71.2)	.007
N stage	0	69 (63.9)	66 (52.8)	
	1-2	39 (36.1)	59 (47.2)	.110
CEA (ng/mL)	≤5	75 (69.4)	51 (40.8)	
	5-15	25 (23.2)	36 (28.8)	
	≥15	8 (7.4)	38 (30.4)	<.001
Operative method	Laparoscopic	41 (38.0)	55 (44.0)	
	Open	67 (62.0)	70 (56.0)	.423

Note: Data are shown as n (%) unless otherwise indicated.
Abbreviation: CEA, carcinoembryonic antigen.

FDFT1 was upregulated in colon cancer cell lines, including Caco2, HCT116, HCT15, HT29, LoVo, RKO, SW480 and SW620, and higher than that in human colon mucosal epithelial cell line (NCM460; Figure 1F). These results suggest that FDFT1 is upregulated in COAD tissues and cell lines.

3.2 | Upregulation of FDFT1 was associated with poor prognosis in stage I-III COAD

Within the follow-up period, there were 73 (31.3%) deaths and 77 (33.0%) tumor relapses. As shown in Table 2, by Kaplan-Meier analysis, seven of the nine variables were found to be associated with patient prognosis (all $P < .05$). Further multivariate analysis with backward elimination identified that age, differentiation grade, T stage, N stage, CEA level, and FDFT1 were independent prognostic factors for both OS and RFS (all $P < .05$). Patients with FDFT1 high expression showed increased risk of death (HR = 3.82; 95% CI, 1.74-8.39; $P < .001$) and relapse (HR = 4.44; 95% CI, 2.06-9.59; $P < .001$). Moreover, these patients had significantly lower OS and RFS rates than those with FDFT1 low expression (both log-rank $P < .001$; Figure 2A,F). In the subgroup analysis by tumor location, the effects existed in the right-sided (Figure 2B,C) and left-sided (Figure 2G,H) COAD. To further evaluate the prognostic value of FDFT1, two prognostic nomograms were constructed based on the six independent predictors. The total scores were calculated by taking the sum of the points from all predictors (Figure 2D,I). Receiver operating characteristic analysis indicated that the nomograms performed well at predicting 5-year OS and RFS, with AUC values of 0.871 and 0.863, respectively (Figure 2E,J). These results indicate that FDFT1 is a prognostic marker in stage I-III COAD.

3.3 | Squalene synthase deficiency attenuated proliferation of HCT116 and HT29 cells

To explore the function of FDFT1 in COAD, we generated HCT116 and HT29 stable cell lines with FDFT1 KD through shRNA interference. The results showed that the endogenous FDFT1 was effectively knocked down (Figure 3A,B). The experiment results from counting cell numbers and EdU staining suggested that FDFT1 KD in HCT116 and HT29 cells significantly inhibited cell proliferation (Figure 3C-F). In addition, FDFT1 KD remarkably suppressed colony formation of HCT116 and HT29 cells (Figure 3G,H). To further investigate the effect of FDFT1 on colon cancer cell proliferation, we also generated FDFT1 overexpressing HT29 and HCT116 stable cell lines using lentivirus. As shown in Figure 3I,J, we separately overexpressed FDFT1 in HCT116 and HT29 cells, and detected the expression level of FDFT1 by western blot analysis. The results showed that FDFT1 was overexpressed in both HCT116 and HT29 cells. Overexpression of FDFT1 promoted colony formation of HCT116 and HT29 cells (Figure 3K,L).

Moreover, we generated another two siRNAs of FDFT1, which clearly reduced expression of FDFT1 in HT29, LoVo, and HCT116

TABLE 2 Univariate and multivariate analyses for overall survival (OS) and relapse-free survival (RFS) in patients with stage I-III colon adenocarcinoma

	OS, univariate	0S, multivariate		RFS, univariate	RFS, multivariate	
Variable	Log-rank *P* value	HR (95% CI)	Log-rank *P* value	Log-rank *P* value	HR (95% CI)	Log-rank *P* value
Age (y)						
≤70 vs. >70	<.001	6.80 (3.15-14.69)	<.001	<.001	5.16 (2.47-10.79)	<.001
Gender						
Male vs. female	.323	—	—	.185	—	—
Tumor location						
Right-sided vs. left-sided	.001	—	—	.003	—	—
Differentiation grade						
Well/moderate vs. poor/mucinous	<.001	2.35 (1.03-5.43)	.045	<.001	2.20 (1.06-5.00)	.047
T stage						
1-3 vs. 4	.005	2.39 (1.07-5.35)	.033	.002	2.85 (1.29-6.31)	.010
N stage						
0 vs. 1-2	.006	1.50 (1.08-3.15)	.042	.008	1.29 (1.06-2.66)	.044
CEA (ng/mL)						
≤5	—	1.00 (reference)	—	—	1.00 (reference)	—
5-15	<.001	3.98 (1.70-9.33)	.002	<.001	3.64 (1.59-8.30)	.002
≥15	<.001	6.62 (2.56-17.10)	<.001	<.001	6.28 (2.47-15.96)	<.001
Operative method						
Open vs. laparoscopic	.433	—	—	.521	—	—
FDFT1						
Low vs. high expression	<.001	3.82 (1.74-8.39)	<.001	<.001	4.44 (2.06-9.59)	<.001

Abbreviations: —, not included in analysis; CEA, carcinoembryonic antigen; CI, confidence interval; FDFT1, squalene synthase; HR, hazard ratio.

cells. Due to the unknown compensation, these two siRNAs did not work well in HCT15 cells. The results showed that FDFT1 KD significantly inhibited cell proliferation and destroyed the cell cycle of HT29, LoVo, and HCT116 cells (Figure S1). The changes in S phase of HT29 and HCT116 cells were different from EdU staining of FDFT1 KD stable cell line (Figure 3E,F), which might account for the transient transfection of siRNAs. However, reducing expression of FDFT1 did not induce apoptosis in these colon cancer cells (Figure S2). The apoptosis rates were less than 10% or around 10%. Taken together, these results suggest that FDFT1 promotes proliferation of colon cancer cells.

3.4 | Downregulation of FDFT1 induced accumulation of NAT8 and D-pantethine to reduce ROS levels and restrain proliferation of HT29 cells

To investigate the molecular mechanism by which FDFT1 promotes colon cancer cell proliferation, we used RNA sequencing and untargeted metabolomics for shControl and FDFT1 KD HT29 cells, respectively (Figure 4A,B). The upregulated genes and metabolites were ranked according to the fold change, *P* value less than .05 (Tables S1 and S2). By analyzing these relative data, we found NAT8 and D-pantethine were obviously upregulated by KD of FDFT1 (Figure 4C,D) with $\log_2$(fold change) of 4.899 and 5.849, respectively. Kyoto Encyclopedia of Genes and Genomes pathway analysis revealed that NAT8 and D-pantethine were involved in glutathione metabolism. *N*-acetyltransferase 8 produces mercapturic acids from acetyl-CoA and cysteine S-conjugates through acetylation.[22] D-pantethine acts as an intermediate in the production of CoA, which then produces acetyl-CoA (Figure 4E).

The glutathione metabolism pathway is controlled by oxidative stress.[23] High levels of ROS stimulate tumorigenesis through promoting cancer cell proliferation.[24] To verify the glutathione metabolism modified by FDFT1, we examined the level of ROS. The data showed that KD of FDFT1 reduced the ROS level of HT29 cells, and ROS scavenger *N*-acetyl-L-cysteine eliminated this difference (Figures 4F and S3A). In addition, supplementation of D-pantethine and overexpression of NAT8 did not further lower the ROS level in FDFT1 KD HT29 cells (Figure S3B-D).

In order to assess the roles of NAT8 and D-pantethine in promoting colon cancer cell proliferation by FDFT1, we overexpressed NAT8 or added D-pantethine in shControl and FDFT1 KD HT29 cells. The expression of endogenous NAT8 is very low and western blot results showed that the exogenous NAT8 was indeed overexpressed in shControl and FDFT1 KD HT29 cells. Moreover, we

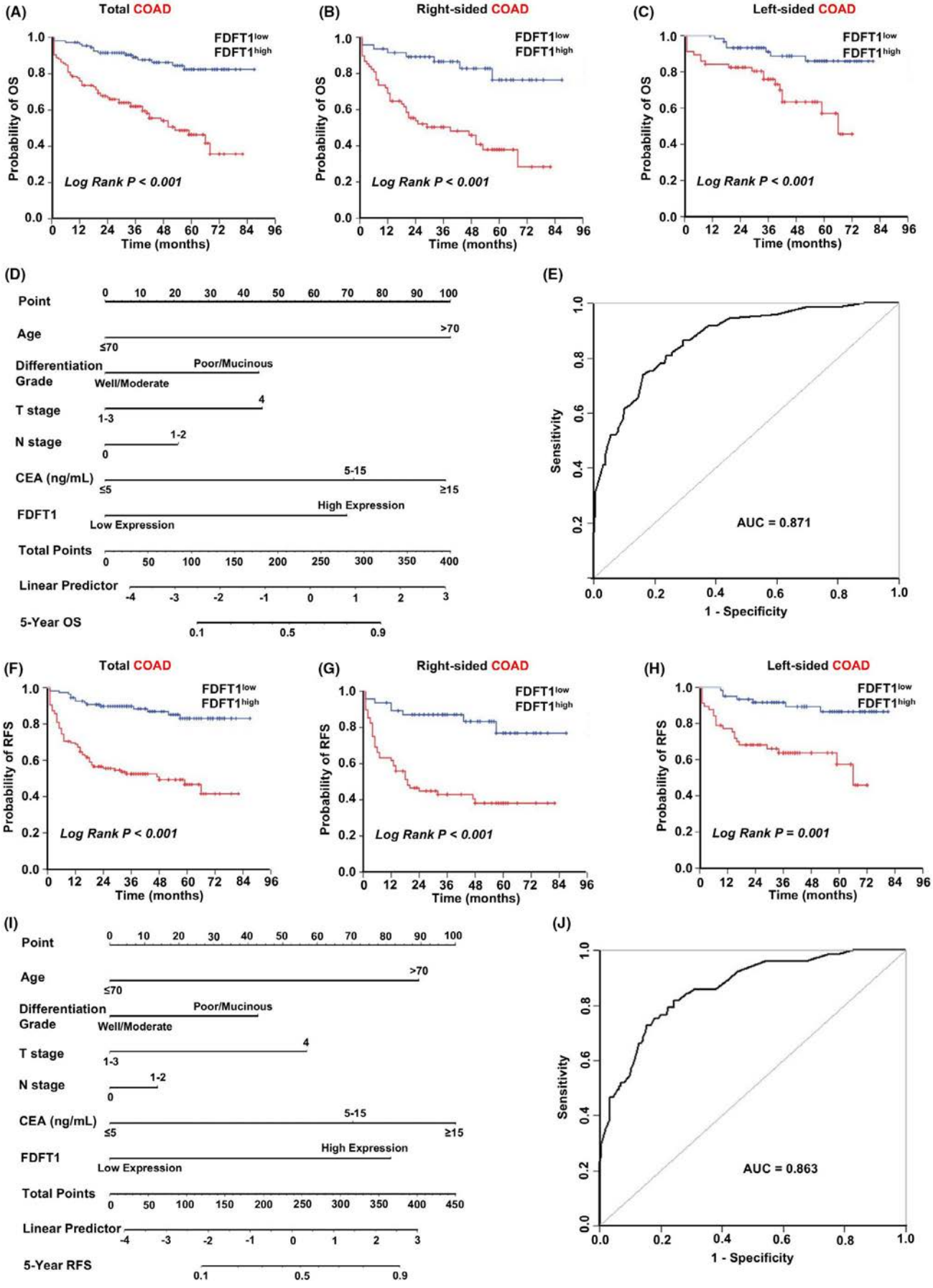

FIGURE 2 Legend on next page

FIGURE 2 Upregulation of squalene synthase (FDFT1) was associated with poor prognosis in stage I-III colon adenocarcinoma (COAD). A, Kaplan-Meier curve for overall survival (OS) according to FDFT1 expression in 233 cases of stage I-III COAD. FDFT1 high expression indicated a lower OS rate (log-rank $P < .001$). B, C, Kaplan-Meier curves for OS according to FDFT1 expression in 115 and 118 cases of right- and left-sided COAD, respectively. FDFT1 high expression indicated a lower OS rate (both log-rank $P < .001$). D, Nomogram for predicting 5-year OS of stage I-III COAD. CEA, carcinoembryonic antigen. E, Receiver operating characteristic (ROC) analysis of the nomogram for predicting 5-year OS (area under the ROC curve [AUC] = 0.871). F, Kaplan-Meier curve for relapse-free survival (RFS) according to FDFT1 expression in 233 cases of stage I-III COAD. FDFT1 high expression indicated a lower RFS rate (log-rank $P < .001$). G, H, Kaplan-Meier curves for RFS according to FDFT1 expression in 115 and 118 cases of right- and left-sided COAD, respectively. FDFT1 high expression indicated a lower RFS rate (log-rank $P < .001$ and $P = .001$, respectively). I, Nomogram for predicting 5-year RFS of stage I-III COAD. J, ROC analysis of the nomogram for predicting 5-year RFS (AUC = 0.863)

found that the increased NAT8 itself was degraded much more in FDFT1 KD HT29 cells than in shControl HT29 cells (Figure 4G). The stabilization of NAT8 could be beneficial for the function of NAT8, which remains to be further explored. The following experiments showed that overexpression of NAT8 inhibited cell proliferation and colony formation of shControl HT29 cells compared to FDFTI KD HT29 cells (Figure 4H-J). Under the supplementation condition of D-pantethine, similar results were observed (Figure 4K,L). These findings indicate that FDFT1 stimulates the increase in ROS level and promotes cell proliferation through reduction of NAT8 and D-pantethine in HT29 cells.

3.5 | Squalene synthase synergized SQLE to accelerate proliferation of colon cancer cells in vitro and in vivo

In our previous study, we found that SQLE promoted colon cancer cell proliferation in vitro and in vivo.[25] Squalene synthase functions upstream of SQLE in the steroid synthesis pathway. Accordingly, we generated the FDFT1/SQLE double-KD HT29 cell line to explore the possibility of the combined functions of FDFT1 and SQLE on colon cancer cell proliferation. The expressions of FDFT1 and SQLE were lower in FDFT1/SQLE KD HT29 cells than in shControl HT29 cells (Figure 5A). The result showed that double KD of FDFT1 and SQLE inhibited colony formation of HT29 cells much more substantially than single KD of FDFT1 or SQLE (Figure 5B,C). However, compared with shControl HT29 cells, the level of cholesterol in FDFT1/SQLE KD HT29 cells was as low as in FDFT1 KD or SQLE KD HT29 cells (Figure 5D).

To further investigate the synergistic function of FDFT1 and SQLE on colon cancer cell proliferation, the FDFT1 inhibitor lapaquistat and the SQLE inhibitor terbinafine were applied. Lapaquistat is a drug for the treatment of hypercholesterolemia, which lowers low-density lipoprotein cholesterol.[26] Terbinafine is used to treat superficial mycosis, and is now being considered as a cancer treatment. Terbinafine induces cell cycle arrest and apoptosis and inhibits angiogenesis in tumor cells.[27-29] Both EdU and colony formation assays showed that combined use of lapaquistat and terbinafine induced a significantly greater suppressive effect than either single drug (Figure 5E-G). Interestingly, the inhibitory effect of terbinafine on proliferation of HT29 cells was dependent on FDFT1 (Figure S4).

Eventually, we applied the in vivo model for clarifying the synergistic functions of FDFT1 and SQLE on tumor growth. The shControl, FDFT1 KD, SQLE KD, and FDFT1/SQLE KD HT29 cells were injected into the left flank of nude mice to monitor tumor formation. Double KD of FDFT1 and SQLE reduced the size and weight of xenograft tumors much more than single KD of FDFT1 or SQLE (Figure 5H-J). Consistent with these observations, the number of Ki-67-positive cells in tumors derived from FDFT1/SQLE double KD HT29 cells was obviously lower than in tumors derived from FDFT1 single KD or SQLE single KD HT29 cells, in the contrast to the control group (Figure 5K,L). We also detected the expression of NAT8 in xenograft tumors. Compared with the shControl group, NAT8 was upregulated in tumors derived from FDFT1 KD HT29 cells (Figure 5M). Collectively, these findings suggest that targeting both FDFT1 and SQLE is more effective for suppressing colon cancer proliferation and tumor progression than sole inhibition of FDFT1 or SQLE.

4 | DISCUSSION

Impairing cancer cell proliferation plays an important role in cancer therapy. In this study, we discovered that FDFT1 served as a prognosis marker in stage I-III COAD and promoted colon cancer cell proliferation. Lack of FDFT1 reduced ROS levels and suppressed colon cancer cell proliferation through upregulation of NAT8 and D-pantethine. Moreover, dual inhibition of FDFT1 and SQLE exerted more antitumor effect than sole inhibition of FDFT1 or SQLE (Figure 6).

Squalene synthase is one of the key regulatory components of the cholesterol biosynthesis pathway. Of particular interest, FDFT1 has been implicated in certain types of cancers, acting as a potential oncogene.[18,30] In the present study, by IHC analysis, FDFT1 was found highly expressed in stage I-III COAD tissues, and its high expression was closely related to the features of aggressive tumors, such as poor differentiation, increased tumor stage, and high CEA level, suggesting an oncogenic role. This study also indicated that FDFT1 high expression was significantly associated with increased risk of tumor recurrence and reduced survival, as shown by multivariate Cox analysis. We noted that a recent study reported that FDFT1 expression was downregulated in colorectal cancer, and the high expression of FDFT1 was associated with favorable prognosis compared with low expression in colorectal cancer.[31] We thought this difference was mainly due to the different composition of the study population. The subjects included in that study were patients with colorectal cancers from

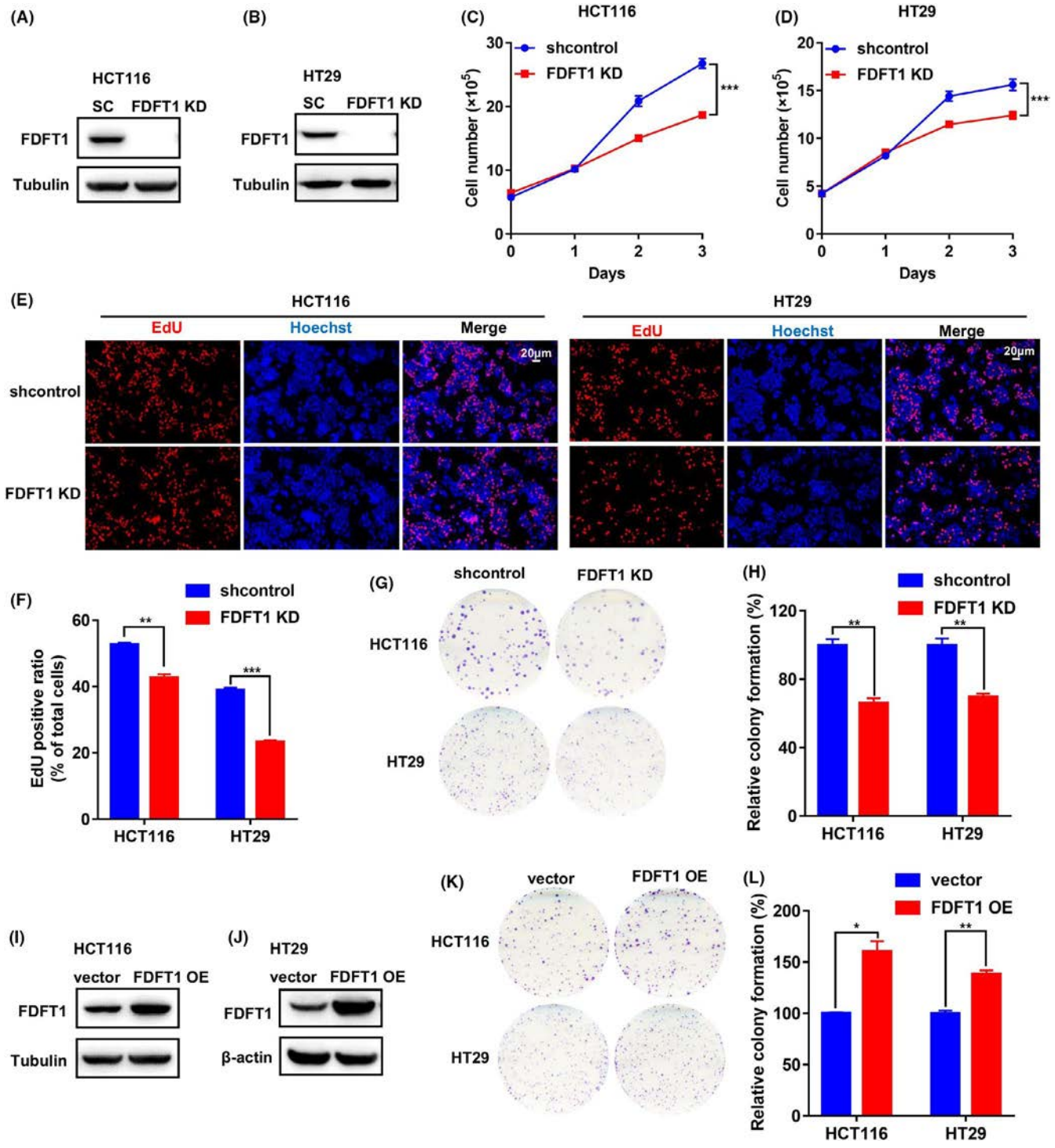

FIGURE 3 Squalene synthase (FDFT1) deficiency attenuated proliferation of HCT116 and HT29 colon cancer cells. A, B, After knockdown (KD) of FDFT1, the protein level of FDFT1 in HCT116 or HT29 cells was detected by western blot analysis; shcontrol (SC) as control group. C, D, After KD of FDFT1, the proliferation of HCT116 or HT29 cells was measured by counting cell numbers. E, After KD of FDFT1, the proliferation of HCT116 or HT29 cells was measured by EdU staining. F, Statistical results of (E). G, Colony formation of HCT116 or HT29 cells was examined by crystal violet staining after KD of FDFT1. H, Statistical results of (G). I, J, After separate overexpression (OE) of FDFT1 in HCT116 or HT29 cells, the protein level of FDFT1 was detected by western blot analysis; vector as control group. K, Colony formation of HCT116 cells or HT29 cells was examined by crystal violet staining after OE of FDFT1. L, Statistical results of (K). Mean ± SEM. $^{*}P < .05$; $^{**}P < .01$; $^{***}P < .001$; ns, no significance

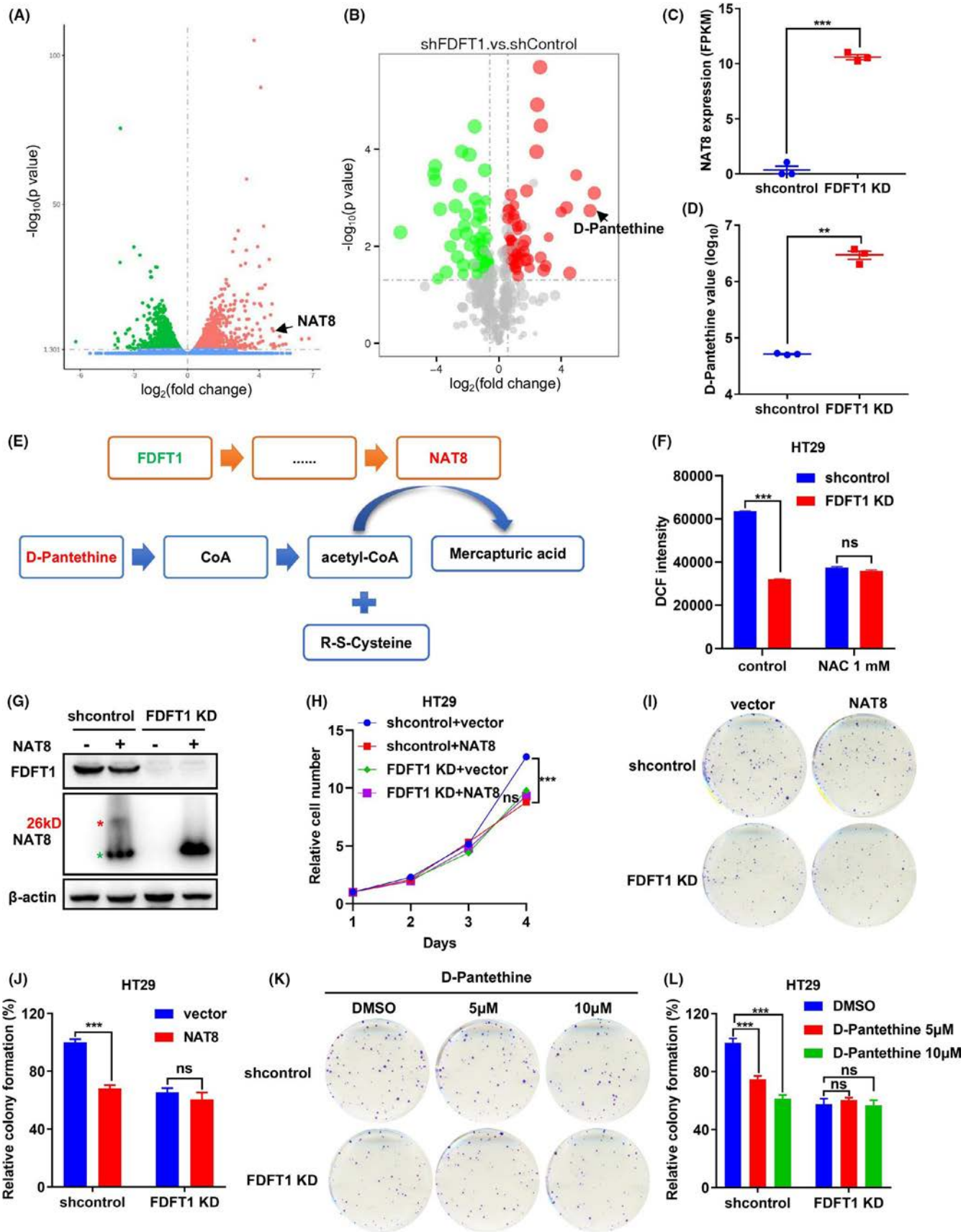
(A)
-log10(p value)
log2(fold change)
NAT8
(B)
shFDFT1.vs.shControl
-log10(p value)
log2(fold change)
D-Pantethine
(C)
NAT8 expression (FPKM)
shcontrol FDFT1 KD
(D)
D-Pantethine value (log10)
shcontrol FDFT1 KD
(E)
FDFT1
.....
NAT8
D-Pantethine
CoA
acetyl-CoA
Mercapturic acid
R-S-Cysteine
(F)
HT29
shcontrol
FDFT1 KD
DCF intensity
control
NAC 1 mM
(G)
shcontrol FDFT1 KD
NAT8
FDFT1
26kD NAT8
β-actin
(H)
HT29
shcontrol+vector
shcontrol+NAT8
FDFT1 KD+vector
FDFT1 KD+NAT8
Relative cell number
Days
(I)
vector
NAT8
shcontrol
FDFT1 KD
(J)
HT29
vector
NAT8
Relative colony formation (%)
shcontrol
FDFT1 KD
(K)
D-Pantethine
DMSO
5μM
10μM
shcontrol
FDFT1 KD
(L)
HT29
DMSO
D-Pantethine 5μM
D-Pantethine 10μM
Relative colony formation (%)
shcontrol
FDFT1 KD

FIGURE 4 Knockdown (KD) of squalene synthase (FDFT1) induced accumulation of *N*-acetyltransferase 8 (NAT8) and D-pantethine to reduce reactive oxygen species level and inhibit proliferation of HT29 cells. A, Volcano plots of RNA sequencing analysis between shControl and FDFT1 KD HT29 cells; 1940 genes were upregulated, and 1828 genes were downregulated. Arrow indicates NAT8. B, Volcano plots of untargeted metabolomics analysis between shControl and FDFT1 KD HT29 cells. Arrow indicates D-pantethine. C, Fragments per kilobase of transcript per million mapped reads (FPKM) value of NAT8 in shControl and FDFT1 KD HT29 cells from (A). D, Value of D-pantethine in shControl and FDFT1 KD HT29 cells from (B). E, Schematic diagram of FDFT1 regulating NAT8 and D-pantethine. Red boxes represent genes; blue boxes represent metabolites. Downregulation of FDFT1 (green) leads to upregulation of NAT8 and D-pantethine (red). F, shControl and FDFT1 KD HT29 cells were pretreated with 1 mmol L^{-1} *N*-acetyl-l-cysteine NAC for 1 h, then analyzed by flow cytometry through DCFH-DA staining. G, NAT8 was overexpressed in shControl and FDFT1 KD HT29 cells. Protein levels of FDFT1 and NAT8 (red star) were detected by western blot analysis; β-actin as a loading control. Green star indicates degradation of NAT8. H-J, Cell proliferation and colony formation of these cells were measured by counting cell numbers and crystal violet staining. K, L, shControl and FDFT1 KD HT29 cells were treated with D-pantethine at concentrations of 0, 5, 10 μmol L^{-1}, respectively, then stained by crystal violet. Mean ± SEM. $^{*}P < .05$; $^{**}P < .01$; $^{***}P < .001$; ns, no significance

stage I to IV; in our study, only patients with stage I-III COAD were enrolled. The FDFT1 expression was upregulated in COAD tumor tissues compared with normal tissues from the Gene Expression Profiling Interactive Analysis database, which indicates that FDFT1 promotes colon cancer progression. We further established two nomograms based on FDFT1 for patients with stage I-III COAD, which showed excellent predictive performance with an AUC of 0.871 for OS and 0.863 for RFS. Our nomograms might provide a more individualized and effective tool for clinicians in therapeutic decision-making and patient counseling.[32]

A previous study reported that FDFT1 was downregulated in colon cancer cell lines.[31] We also detected FDFT1 mRNA expression in colon cancer cell lines by RT-PCR analysis. Using *β-actin* rather than *GAPDH* as a housekeeping gene, the expression of FDFT1 was upregulated in colon cancer cell lines compared to NCM460 cells (Figure 1F). We think *GAPDH* might not be a good reference gene because FDFT1 regulates the metabolism pathway. In HT29 cells, KD of FDFT1 indeed inhibited cell proliferation and further enhanced the antitumor effect of SQLE inhibition. The function of FDFT1 in COAD remains to be further verified by establishing an orthotopic tumor model or generating FDFT1 transgenic mice.

In addition, FDFT1 deficiency not only reduced the level of cholesterol as well as SQLE, but also upregulated NAT8 and D-pantethine. Both NAT8 and D-pantethine lead to the formation of mercapturic acids, which biotransform xenobiotic and endobiotic electrophilic compounds and their metabolites.[33] Knockdown of FDFT1 might activate this detoxication reaction to suppress colon cancer cell proliferation. Additionally, NAT8 and D-pantethine are involved in glutathione metabolism, which influences the level of ROS. The decreasing ROS level in FDFT1 KD HT29 cells could contribute to inhibiting the oncogenic signaling pathway. However, the link between FDFT1 and ROS remains to be further researched.

Combined use of the FDFT1 inhibitor lapaquistat and the SQLE inhibitor terbinafine effectively inhibited colon cancer cell proliferation in vitro, which should be further confirmed by in vivo experiments. The targeted inhibitors of FDFT1 or SQLE also should be optimized with the substitution of other more novel compounds.[30]

5 | CONCLUSIONS

Overall, our study provides the insight that FDFT1 acts as a valuable prognostic marker in stage I-III COAD and synergizes SQLE to promote colon cancer cell proliferation. The dual inhibition of FDFT1 and SQLE is a new therapy for stage I-III COAD.

ACKNOWLEDGMENTS

We thank the molecular biology technology platform, cell analysis technology platform, chemical biology technology platform and animal experiment technology platform in the CAS Center for Excellence in Molecular Cell Science. We appreciate the clinical research and translational medicine center of Yangpu Hospital for offering COAD samples. This work was supported by the National Natural Science Foundation of China (No. 81874201), Shanghai Municipal Health Bureau (No. ZK2019A19), Science and Technology Commission of Shanghai Municipality (No. 19411971500), Shanghai Pujiang Program (No. 21PJD066) and The National Key

FIGURE 5 Combined inhibition of squalene synthase (FDFT1) and squalene epoxidase (SQLE) suppressed growth of colon cancer cells and xenograft tumors. A, After separate or double knockdown (KD) of FDFT1 and SQLE, the protein levels of FDFT1 and SQLE in HT29 cells were detected by western blot analysis; shControl, control group. B, Colony formation of cells in (A) were measured by crystal violet staining. C, Statistical results of (B). D, Intracellular total cholesterol level of shControl, FDFT1 KD, SQLE KD, and FDFT1/SQLE HT29 cells were measured. E, HT29 cells were treated with lapaquistat (La) and terbinafine (Te) at different concentrations for 48 or 72 h, then stained with EdU. F, After combined treatment with La and Te, the colony formation of HCT116 and HT29 cells was measured by crystal violet staining. G, Statistical results of (F). H, Tumor growth of shControl, FDFT1 KD, SQLE KD, and FDFT1/SQLE KD HT29 cells in nude mice after injection for 1 wk. I, J, Images and weights of the tumors in (H) removed from nude mice. K, Immunohistochemical analysis of Ki-67 in xenograft tumors from (I). Scale bars, 50 μm. L, Statistical results of (K). M, FDFT1 and *N*-acetyltransferase 8 (NAT8) mRNA levels in tumors derived from shControl and FDFT1 KD HT29 cells. Mean ± SEM. $^{*}P < .05$, $^{**}P < .01$, $^{***}P < .001$

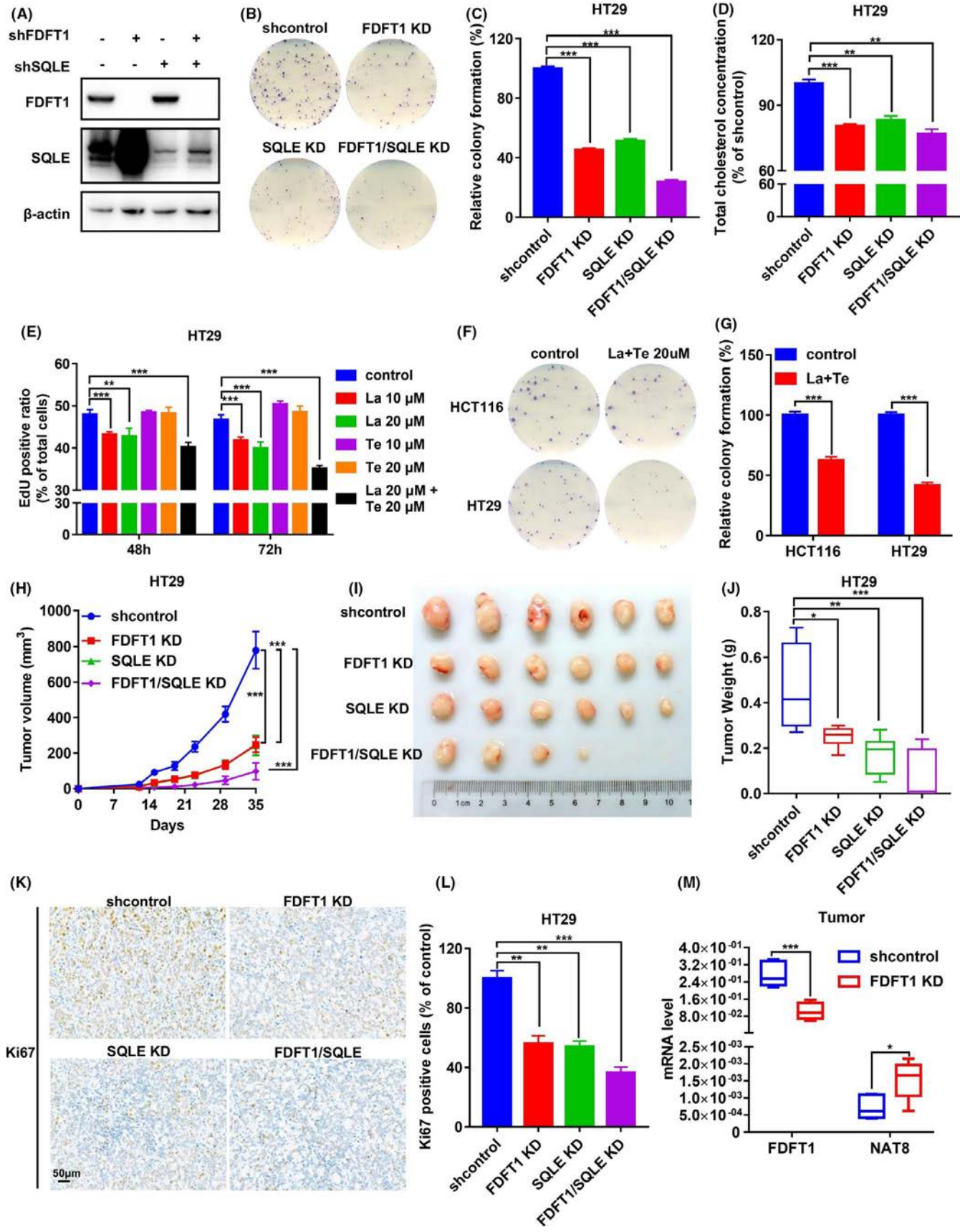
(A)
shFDFT1 - + - +
shSQLE - - + +
FDFT1
SQLE
β-actin
(B)
shcontrol
FDFT1 KD
SQLE KD
FDFT1/SQLE KD
(C)
HT29
Relative colony formation (%)
shcontrol
FDFT1 KD
SQLE KD
FDFT1/SQLE KD
(D)
HT29
Total cholesterol concentration (% of shcontrol)
(E)
HT29
EdU positive ratio (% of total cells)
48h
72h
control
La 10 μM
La 20 μM
Te 10 μM
Te 20 μM
La 20 μM + Te 20 μM
(F)
control
La+Te 20uM
HCT116
HT29
(G)
control
La+Te
Relative colony formation (%)
HCT116
HT29
(H)
HT29
Tumor volume (mm3)
shcontrol
FDFT1 KD
SQLE KD
FDFT1/SQLE KD
Days
(I)
shcontrol
FDFT1 KD
SQLE KD
FDFT1/SQLE KD
(J)
HT29
Tumor Weight (g)
(K)
shcontrol
FDFT1 KD
SQLE KD
FDFT1/SQLE
Ki67
50μm
(L)
HT29
Ki67 positive cells (% of control)
(M)
Tumor
mRNA level
shcontrol
FDFT1 KD
FDFT1
NAT8

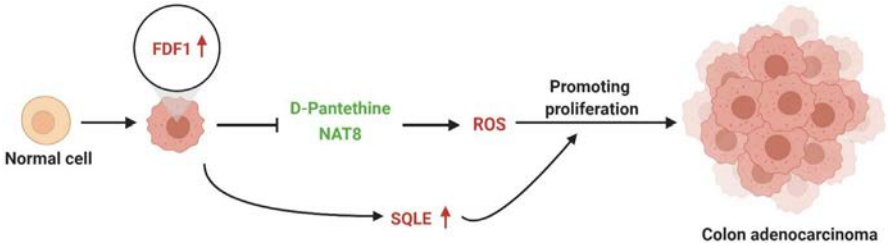

FIGURE 6 Schematic diagram showing synergistic function of squalene synthase (FDFT1) and squalene epoxidase (SQLE) in promoting colon adenocarcinoma (COAD). FDFT1 induces accumulation of reactive oxygen species (ROS) level and promotes colon cancer cell proliferation through upregulation of D-pantethine and *N*-acetyltransferase 8 (NAT8). FDFT1 also synergizes SQLE to facilitate COAD progression

Research and Development Program of China (2020YFA0509000, 2017YFA0503600).

CONFLICT OF INTEREST

The authors declare that they have no competing interests.

ETHICAL APPROVAL AND CONSENT TO PARTICIPATE

The study was reviewed and approved by the Local Ethics Committee of Yangpu Hospital affiliated to Tongji University School of Medicine (LL-2021-SCI-004). All of the enrolled patients signed informed consent forms.

DATA AVAILABILITY STATEMENT

The RNA sequencing data have been submitted to Sequence Read Archive (SRA). BioProject ID: PRJNA738852, http://www.ncbi.nlm.nih.gov/bioproject/738852; BioProject ID: PRJNA737171, http://www.ncbi.nlm.nih.gov/bioproject/737171; BioProject ID: PRJNA737203, http://www.ncbi.nlm.nih.gov/bioproject/737203. The untargeted metabolomics data have been submitted to MetaboLights, http://www.ebi.ac.uk/metabolights/MTBLS2937; https://www.ebi.ac.uk/metabolights/MTBLS2966. The data that support the findings of this study are available from the corresponding authors upon reasonable request.

ORCID

Moubin Lin https://orcid.org/0000-0001-7466-3315
Luwei He https://orcid.org/0000-0001-6564-848X

REFERENCES

1. Siegel RL, Miller KD, Fuchs HE, Jemal A. Cancer statistics, 2021. *CA Cancer J Clin*. 2021;71:7-33.
2. Sung H, Ferlay J, Siegel RL, et al. Global cancer statistics 2020: GLOBOCAN estimates of incidence and mortality worldwide for 36 cancers in 185 countries. *CA Cancer J Clin*. 2021;71:209-249.
3. Siegel RL, Miller KD, Goding Sauer A, et al. Colorectal cancer statistics, 2020. *CA Cancer J Clin*. 2020;70:145-164.
4. Tjandra JJ, Chan MK. Follow-up after curative resection of colorectal cancer: a meta-analysis. *Dis Colon Rectum*. 2007;50:1783-1799.
5. Yang IP, Tsai HL, Hou MF, et al. MicroRNA-93 inhibits tumor growth and early relapse of human colorectal cancer by affecting genes involved in the cell cycle. *Carcinogenesis*. 2012;33:1522-1530.
6. Quirke P, Williams GT, Ectors N, Ensari A, Piard F, Nagtegaal I. The future of the TNM staging system in colorectal cancer: time for a debate? *Lancet Oncol*. 2007;8:651-657.
7. Peng F, Huang Y, Li MY, et al. Dissecting characteristics and dynamics of differentially expressed proteins during multistage carcinogenesis of human colorectal cancer. *World J Gastroenterol*. 2016;22:4515-4528.
8. Jakopovic B, Horvatić A, Klobučar M, et al. Treatment With medicinal mushroom extract mixture inhibits translation and reprograms metabolism in advanced colorectal cancer animal model as evidenced by tandem mass tags proteomics analysis. *Front Pharmacol*. 2020;11:1202.
9. Guinney J, Dienstmann R, Wang X, et al. The consensus molecular subtypes of colorectal cancer. *Nat Med*. 2015;21:1350-1356.
10. Zhang L, Theodoropoulos PC, Eskiocak U, et al. Selective targeting of mutant adenomatous polyposis coli (APC) in colorectal cancer. *Sci Transl Med*. 2016;8:361ra140.
11. Wen YA, Xiong X, Zaytseva YY, et al. Downregulation of SREBP inhibits tumor growth and initiation by altering cellular metabolism in colon cancer. *Cell Death Dis*. 2018;9:265.
12. Tsoi H, Chu ESH, Zhang X, et al. Peptostreptococcus anaerobius induces intracellular cholesterol biosynthesis in colon cells to induce proliferation and causes dysplasia in mice. *Gastroenterology*. 2017;152(1419–1433):e1415.
13. Cheung K-S, Chen L, Chan EW, Seto W-K, Wong ICK, Leung WK. Statins reduce the progression of non-advanced adenomas to colorectal cancer: a postcolonoscopy study in 187 897 patients. *Gut*. 2019;68:1979.
14. Kodach LL, Jacobs RJ, Voorneveld PW, et al. Statins augment the chemosensitivity of colorectal cancer cells inducing epigenetic reprogramming and reducing colorectal cancer cell 'stemness' via the bone morphogenetic protein pathway. *Gut*. 2011;60:1544-1553.
15. Do R, Kiss RS, Gaudet D, Engert JC. Squalene synthase: a critical enzyme in the cholesterol biosynthesis pathway. *Clin Genet*. 2009;75:19-29.
16. Pandit J, Danley DE, Schulte GK, et al. Crystal structure of human squalene synthase. A key enzyme in cholesterol biosynthesis. *J Biol Chem*. 2000;275:30610-30617.
17. Liu C-I, Jeng W-Y, Chang W-J, Shih M-F, Ko T-P, Wang AHJ. Structural insights into the catalytic mechanism of human squalene synthase. *Acta Crystallogr D Biol Crystallogr*. 2014;70:231-241.
18. Tüzmen Ş, Hostetter G, Watanabe A, et al. Characterization of farnesyl diphosphate farnesyl transferase 1 (FDFT1) expression in cancer. *Per Med*. 2019;16:51-65.
19. Brusselmans K, Timmermans L, Van de Sande T, et al. Squalene synthase, a determinant of raft-associated cholesterol and modulator of cancer cell proliferation. *J Biol Chem*. 2007;282:18777-18785.

20. Yang YF, Chang YC, Jan YH, Yang CJ, Huang MS, Hsiao M. Squalene synthase promotes the invasion of lung cancer cells via the osteopontin/ERK pathway. *Oncogenesis*. 2020;9:78.
21. Yang YF, Jan YH, Liu YP, et al. Squalene synthase induces tumor necrosis factor receptor 1 enrichment in lipid rafts to promote lung cancer metastasis. *Am J Resp Crit Care*. 2014;190:675-687.
22. Veiga-da-Cunha M, Tyteca D, Stroobant V, Courtoy PJ, Opperdoes FR, Van Schaftingen E. Molecular identification of NAT8 as the enzyme that acetylates cysteine S-conjugates to mercapturic acids. *J Biol Chem*. 2010;285:18888-18898.
23. Sies H, Berndt C, Jones DP. Oxidative stress. *Annu Rev Biochem*. 2017;86:715-748.
24. Hayes JD, Dinkova-Kostova AT, Tew KD. Oxidative stress in cancer. *Cancer Cell*. 2020;38:167-197.
25. He L, Li H, Pan C, et al. Squalene epoxidase promotes colorectal cancer cell proliferation through accumulating calcitriol and activating CYP24A1-mediated MAPK signaling. *Cancer Commun (Lond)*. 2021;41(8):726-746.
26. Stein EA, Bays H, O'Brien D, Pedicano J, Piper E, Spezzi A. Lapaquistat acetate development of a squalene synthase inhibitor for the treatment of hypercholesterolemia. *Circulation*. 2011;123:1974-1985.
27. Ho PY, Liang YC, Ho YS, Chen CT, Lee WS. Inhibition of human vascular endothelial cells proliferation by terbinafine. *Int J Cancer*. 2004;111:51-59.
28. Ho PY, Zhong WB, Ho YS, Lee WS. Terbinafine inhibits endothelial cell migration through suppression of the Rho-mediated pathway. *Mol Cancer Ther*. 2006;5:3130-3138.
29. Lee W-S, Chen R-J, Wang Y-J, et al. In vitro and in vivo studies of the anticancer action of terbinafine in human cancer cell lines: G0/G1p53-associated cell cycle arrest. *Int J Cancer*. 2003;106:125-137.
30. Ha NT, Lee CH. Roles of farnesyl-diphosphate farnesyltransferase 1 in tumour and tumour microenvironments. *Cells*. 2020;9(11):2352.
31. Weng ML, Chen WK, Chen XY, et al. Fasting inhibits aerobic glycolysis and proliferation in colorectal cancer via the Fdft1-mediated AKT/mTOR/HIF1alpha pathway suppression. *Nat Commun*. 2020;11:1869.
32. Shariat SF, Capitanio U, Jeldres C, Karakiewicz PI. Can nomograms be superior to other prediction tools? *BJU Int*. 2009;103:492-497. discussion 495–497.
33. Hanna PE, Anders MW. The mercapturic acid pathway. *Crit Rev Toxicol*. 2019;49:819-929.

SUPPORTING INFORMATION

Additional supporting information may be found in the online version of the article at the publisher's website.

How to cite this article: Jiang H, Tang E, Chen Y, et al. Squalene synthase predicts poor prognosis in stage I-III colon adenocarcinoma and synergizes squalene epoxidase to promote tumor progression. *Cancer Sci*. 2022;113:971–985. doi:10.1111/cas.15248